A Practical Method for Butterfly Motion Capture

Qiang Chen
qiangchen@jxufe.edu.cn
Jiangxi University of Finance and Economics
China

Tingsong Lu
tingsonglu@ecjtu.edu.cn
East China Jiaotong University
China

Yang Tong
tongyang@ecjtu.edu.cn
East China Jiaotong University
China

Yuming Fang
fa0001ng@e.ntu.edu.sg
Jiangxi University of Finance and Economics
China

Zhigang Deng*
zdeng4@central.uh.edu
University of Houston
USA

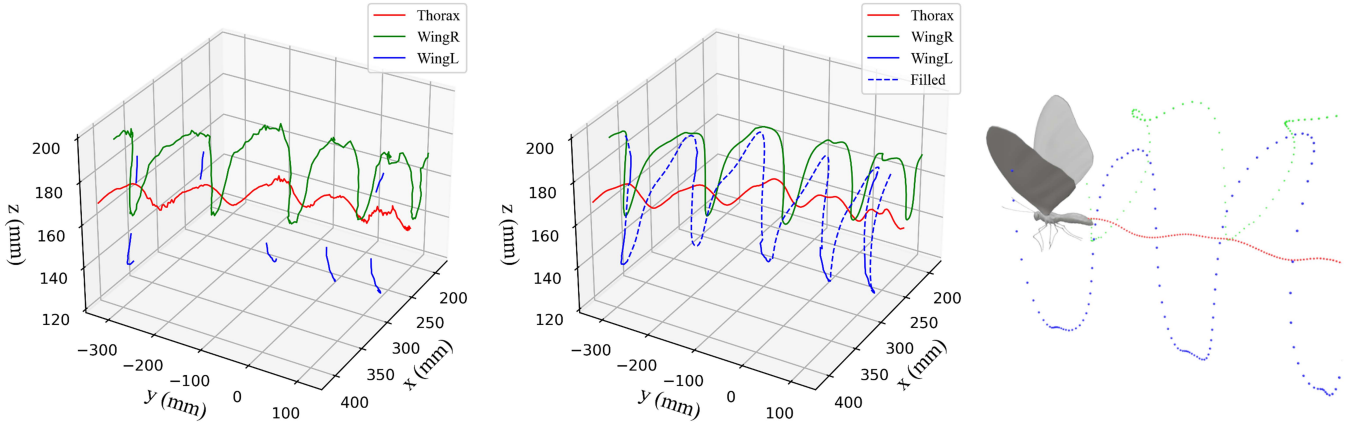

(A) Original **(B) Processed by our method** **(C) Visualization**

Figure 1: The motion-captured trajectories of the thorax and wings of a flying butterfly. (A) The original captured butterfly motion, (B) the butterfly motion processed by our method, and (C) visualization of the obtained butterfly flight motion.

ABSTRACT

Simulating realistic butterfly motion has been a widely-known challenging problem in computer animation. Arguably, one of its main reasons is the difficulty of acquiring accurate flight motion of butterflies. In this paper we propose a practical yet effective, optical marker-based approach to capture and process the detailed motion of a flying butterfly. Specifically, we first capture the trajectories of the wings and thorax of a flying butterfly using optical marker-based motion tracking. After that, our method automatically fills the positions of missing markers by exploiting the continuity and relevance of neighboring frames, and improves the quality of the captured motion via noise filtering with optimized parameter settings. Through comparisons with existing motion processing methods, we demonstrate the effectiveness of our approach to obtain accurate flight motions of butterflies. Furthermore, we created and will release a first-of-its-kind butterfly motion capture dataset to research community.

CCS CONCEPTS

• **Computing methodologies** → **Motion capture**.

KEYWORDS

datasets, motion capture, butterfly

ACM Reference Format:
Qiang Chen, Tingsong Lu, Yang Tong, Yuming Fang, and Zhigang Deng. 2022. A Practical Method for Butterfly Motion Capture. In *ACM SIGGRAPH Conference on Motion, Interaction and Games (MIG '22), November 3–5, 2022, Guanajuato, Mexico.* ACM, New York, NY, USA, 9 pages. https://doi.org/10.1145/3561975.3562940

*corresponding author

MIG '22, November 3–5, 2022, Guanajuato, Mexico

ACM ISBN 978-1-4503-9888-6/22/11…$15.00
https://doi.org/10.1145/3561975.3562940

1 INTRODUCTION

Butterflies with peculiar and beautiful flight motion have been simulated and used in a variety of applications including movies, games, VR/AR, bionic robots, etc. Previously researchers have used various experimental methods to capture butterfly motion. For instance, researchers captured the aerodynamics of a flapping insect through wind tunnels [Johansson and Henningsson 2021; Srygley and Thomas 2002] or tracked the flight trajectories of a flying butterfly using multiple cameras [Guo et al. 2018]. However, such methods are either too expensive (e.g., using wind tunnels) or less useful for graphics applications (e.g., the flight trajectories of a butterfly alone are generally insufficient to create realistic butterfly animations). Indeed, since butterflies with peculiar flight styles are petite in size (far more tiny than bats [Hubel et al. 2009] or birds [Ju et al. 2013]), it is particularly challenging to capture the detailed dynamic motion of their body parts, i.e., wings and thorax, during their flights.

Meanwhile, in computer graphics and animation applications, motion capture has become a standard approach to acquire accurate motion of humans as well as animals. As a result, there exist many large-scale human motion capture datasets publicly available, which have significantly facilitated the booming of numerous MoCap based research advances in recent years. Unfortunately, due to the aforementioned challenge of acquiring detailed butterfly motion, to the best of our knowledge, none of butterfly motion datasets (including the motions of the wings and thorax) exists these days, in particular, for graphics and animation applications. The lack of any publicly available butterfly motion datasets not only limits applying the simulation of butterflies to a variety of entertainment and VR applications, but also hinders the advance of butterfly motion related research in broad scientific communities.

Inspired by the above need, in this paper we propose a practical method to capture motion of a flying butterfly with dynamic details, including the motions of its wings and thorax, using optical marker based motion tracking. We design a set of butterfly-specific motion processing algorithms to automatically recover missing markers and filter out noise from the captured butterfly motion data. Finally, based on our method, we created a butterfly motion capture dataset and will make it publicly available to the research community. Figure 1 show examples of motion-captured trajectories of the thorax and wings of a flying butterfly by our method.

The main contributions of this work can be summarized as follows:

- On top of existing optical marker-based motion tracking technology, we design a practical method to capture and process the detailed dynamic motion of a flying butterfly including the motions of its wings and thorax, via a set of butterfly-specific motion processing and filtering algorithms.
- We created a first-of-its-kind, butterfly motion capture dataset of swallow-tail butterflies (*Papilio polytes*), and will make it publicly available to the research community.

2 RELATED WORK

In this section we only briefly review recent efforts that are related to this work: flying insect motion acquisition, flying insect simulation, and motion capture data processing. For general vision-based motion capture technology, please refer to the well-known survey by Moeslund and Granum [Moeslund and Granum 2001].

Simulation of flying insects and butterflies. Simulation of flying insects including butterflies has caught increasing attention in recent years. Due to the difficulty of acquiring ground-truth motion of flying insects, researchers developed various empirical models to simulate flying insects, including velocity field based methods [Chen et al. 2019; Wang et al. 2014], and biologically inspired methods [Li et al. 2015; Wang et al. 2015]. Xiang et al. [Xiang et al. 2020] proposed a data-driven framework to simulating flying insect swarms based on scarce public fruit fly's motion data [Sinhuber et al. 2019]. However, their method is focused on the generation of flying trajectories of insect swarms, not dynamic motion of individual flying insects. Recently, Chen et al. [Chen et al. 2022] proposed a heuristic model to simulate flying butterflies by introducing parametric maneuvering functions for dynamic motion control.

Flying insect motion acquisition. Due to the well-recognized importance of acquiring ground-truth motion data of flying insects, researchers attempted various ways to record the motion of flying insects. In the early days, sensor systems were used for acquiring the motion of flying insects [Dickinson et al. 1999], but binding insects with sensors is practically difficult and un-robust. In recent years, markerless vision-based tracking methods have started to be used for motion tracking of flying insects. For example, Fry et al. [Fry et al. 2000] use pan-tilt multi-cameras to track a flying honeybee's 3D trajectories. Ristroph et al. [Ristroph et al. 2011] use high-speed cameras to analyze the paddling mode of the forwarding of a fruit fly. Similarly, Koehler et al. [Koehler et al. 2011] capture a dragonfly's motion through high-speed cameras and visualize the flapped vortices based on the captured data. The above markerless vision-based methods generally employ multiple cameras to track the 3D trajectories of flying insects. However, due to the tiny size of flying insects, it is non-trivial, without considerable efforts, to acquire their detailed flight motion, beyond trajectory acquisition.

Researchers also exploited wind tunnels to record the aerodynamics of flapping insects. To obtain the laminar flow around a flapping butterfly, Srygley et al. [Srygley and Thomas 2002] blow smog into a wind tunnel while using a high-speed camera to record digital images. Johansson et al. [Johansson and Henningsson 2021] use a similar method to record the take-off feature of a butterfly and found that the cup-shape deformation of the wings promotes flight effectiveness. Compared to markerless vision-based tracking, the above wind tunnel-based methods in general can achieve accuracy, but they are too expensive and thus practically infeasible for many applications. Also, often it is difficult for them to capture the motion of flying insects at a mid-term distance (for example, > 1 meter) due to the space limitation.

As a trade-off between the above two methods, optical markers have been explored for acquiring flying insect motion. For example, Ju et al. [Ju et al. 2013] use markers to capture the wing flapping of a bird in order to create its simulation model. Sridhar et al. [Sridhar et al. 2016] elaborately place markers on the wings and thorax of a monarch butterfly and then use a motion capture system to track the movements of the markers. However, their work does not provide any technical details on motion acquisition and processing. In addition, somehow they only captured and studied 0.2

second motion data of a flying butterfly, and their dataset has not been released to the research community. Different from [Sridhar et al. 2016], our method can robustly acquire, process, and produce quality motion data of a flying butterfly with a longer duration and thus is more practically effective. Also, based on our method, we created and will release a first-of-its-kind butterfly motion capture dataset that encloses the detailed dynamic motion of butterflies for graphics and animation applications.

Motion capture data processing. Motion capture has been increasingly used for acquiring high quality motion of humans and animals [Bodenheimer et al. 1997; Vlasic et al. 2007]. Here we review some recent works on motion capture data denoising and missing marker handling. Yu et al. [Yu et al. 2007] proposed algorithms to handle missing or contaminated markers in complex mocap data (e.g., multiple interacting articulated targets). Researchers also proposed algorithms for motion capture data denoising [Holden 2018] or for information extraction from sparse marker motion [Loper et al. 2014]. By utilizing existing large-scale human motion capture datasets as the training data, Chen et al. [Chen et al. 2021] developed a deep learning based method for handling noisy and incomplete motion capture data.

3 OUR METHOD

Experimental setup. Our butterfly motion capture experiments were conducted by using a motion capture system with Qualisys cameras and a Qualisys Track Manager (QTM) software [Qualisys 2013] (refer to Figure 2(b)). Before the start of our experiments, we tested the sensing distance between the cameras and optical markers. We found that the acceptable distance is about 1.5 meter when we use the selected markers (described below). Based on the test result, we designed a cylinder-shaped capture volume with 1.0 meter radius and 1.0 meter height (shown in Figure 2(a)). Confined by the limited capture volume, we only use 7 cameras to capture butterfly motion. Furthermore, a green clothing is placed on the floor to reduce the interference of background light, and a mask is used to prevent the escaping of the butterflies inside. The used Oqus 6+ cameras are capable of capturing motion at 1660 fps, with a sensor resolution of 1536 × 992. In this work, we set the capture frequency with 500 fps, which is two orders of magnitude higher than the butterfly' flapping frequency (i.e., about 11 Hz).

Markers selection and placement. Optical markers are covered with a special material that is designed to efficiently reflect invisible infrared light so that cameras can sense it. We tested four different size of optical markers (Marker #1 to #4 shown in Figure 4). The masses and dimensions of the four types of makers are summarized in Table 1. To this end, the hemispherical marker #4 was chosen for butterfly motion capture in this work since it has the smallest dimension among the four options and thus has less impact on butterfly's flight behavior. The butterfly used in our experiments was hatched from chrysalis. The specimen is *papilio polytes* (swallowtail butterfly).

It was previously reported that the forewings play a key role in butterfly flights, whereas the hindwings are less essential [Jantzen and Eisner 2008]. Therefore, in order to capture the natural flight motion of a butterfly with less evasive influence, we only place markers on the forewings and thorax of the butterfly. As shown in Figure 3, a total of five markers are placed on the butterfly including four on the forewings and one on the thorax. The markers are symmetrically placed on both sides of the wings so that they substitute for each other when the marker on one side disappears from the camera's view during flapping. The markers on the forewings denote the flapping motion of the butterfly, and the marker on the thorax mainly provides information on the trajectory of the butterfly body.

Table 1: Features of four types of optical markers

Marker type	Marker #	Dimension (mm)	Mass (g)	% Butterfly mass (0.35 g)
Spherical	1	15	2.122	606.3
	2	4.5	0.076	21.7
Circular (flat)	3	6.5	0.010	2.9
Hemispherical	4	2.5	0.004	1.1

4 BUTTERFLY MOTION DATA PROCESSING

The butterfly motion data directly obtained from the motion capture system is inevitably noisy and often incomplete (with missing markers). The average percentage of missing frames in each captured session is **79.1%**, which imposes a non-trivial technical challenge for butterfly motion data processing and cleaning. To this end, we design a set of butterfly-specific motion processing steps, including missing marker handling, noisy trajectory smoothing, and key parameters optimization, described below.

4.1 Missing Marker Handling

In our butterfly motion capture experiments, there are three possible cases of missing markers: (i) the thorax marker is missing; (ii) the marker on one of the wings is missing; and (iii) the markers on both wings are missing. We describe how we handle the above three cases below.

The thorax marker missing. Based on our experiments, we found that the thorax marker was seldom missing. Then, even when the thorax marker is missing, we directly fill the missing marker through a cubic spline interpolation of the thorax markers at neighboring frames.

Markers on both wings missing. If the markers on both wings are missing in a frame, which rarely happened, we identify the neighboring frames with wing markers and then perform a cubic spline interpolation on them.

Markers on one of the wings missing. Compared to the above two cases, the case where only the markers on one of the wings are missing was observed more frequently in our data. To handle this case, we design an effective algorithm to fill the missing marker, described below.

First, for any frame we define a *reference vertical plane*, which denotes the butterfly with a zero roll angle. As illustrated in Figure 5(a), $\mathbf{r}_{t,*}$ is the thorax marker at a frame and $\mathbf{r}_{t,*+m}$ is the thorax position at the $(*+m)$-th frame. m is the step size. The butterfly's body direction can be approximately determined by $(\mathbf{r}_{t,*+m} - \mathbf{r}_{t,*})$.

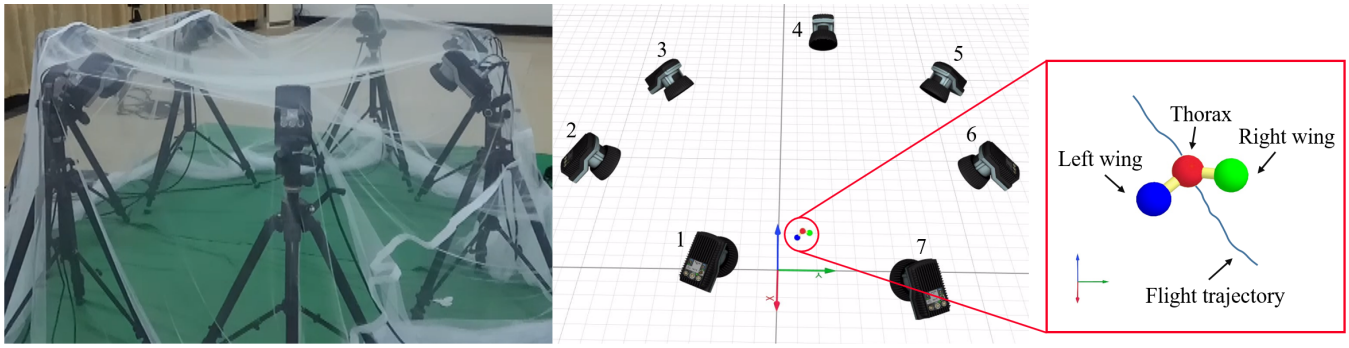

Figure 2: Experimental setup. (*a*) Physical capture volume; (*b*) Virtual capture volume and the cameras placement shown in QTM software. The close up view of the sensed markers on the butterfly.

Figure 3: Markers are circled in red on the dorsal (*a*) and ventral (*b*) side of the butterfly.

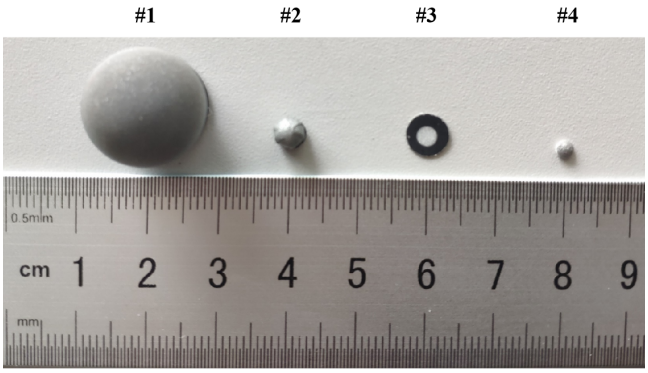

Figure 4: Four types of optical markers were considered for our butterfly motion capture experiments. Marker #4 was used in this work.

$\mathbf{r}_o$ is an auxiliary point and can be calculated as follows:

$$\mathbf{r}_{o,*} = \mathbf{r}_{t,*} + \mathbf{j} \cdot h, \tag{1}$$

where $\mathbf{j}$ is a unit vector along the positive Y-axis in the 3D coordinate system, and h as a scalar value is experimentally set to 10. By using the auxiliary point $\mathbf{r}_o$, we can construct the reference vertical plane with a zero roll angle, and its normal is denoted as $\mathbf{n}_{zero}$.

Furthermore, we also compute another plane, called as the *actual-posture-plane* in this paper. As illustrated in Figure 5(b), $\mathbf{r}_l$ and $\mathbf{r}_r$ are the markers on the left and right wings, respectively. $\mathbf{r}_{mid}$ is the mid point between $\mathbf{r}_l$ and $\mathbf{r}_r$. $\mathbf{n}_{actual}$ denotes the normal of the actual-posture-plane. To this end, a roll angle φ, between $\mathbf{n}_{zero}$ and n_{actual}, can be computed.

If the marker on one of the wings is missing, based on the hypothesis that the bilateral wings of butterflies are symmetric [Dudley 2002], we can fill the missing wing marker with the marker on its opposite wing, with the aid of both $\mathbf{n}_{zero}$ and $\mathbf{n}_{actual}$. Without loss of generality, we assume the marker on the left wing is missing. The missing left wing marker (the red point in Figure 5(c)) at the i-th frame is calculated as follows:

$$\mathbf{r}_{l,i} = \mathbf{r}_{r,i} + 2 \cdot d_i \cdot \frac{\mathbf{n}_{actual,i}}{|\mathbf{n}_{actual,i}|}, \tag{2}$$

where d_i is the distance between the right wing's marker $\mathbf{r}_{r,i}$ and the actual-posture-plane, and it is calculated as follows:

$$d_i = \frac{(\mathbf{r}_{r,i} - \mathbf{r}_{t,i}) \cdot \mathbf{n}_{actual,i}}{|\mathbf{n}_{actual,i}|}. \tag{3}$$

However, because of the lack of the left wing marker, we cannot directly compute $\mathbf{n}_{actual,i}$, but it can be computed with the aid of $\mathbf{n}_{zero,i}$, as follows:

$$\mathbf{n}_{actual} = \mathbf{n}_{zero,i} \cdot \begin{pmatrix} \cos\varphi_i & -\sin\varphi_i & 0 \\ \sin\varphi_i & \cos\varphi_i & 0 \\ 0 & 0 & 1 \end{pmatrix}, \tag{4}$$

where φ_i is obtained through a cubic spline interpolation of the φ_* of fully captured, neighboring frames (refer to Figure 5(b)).

Note the step size m is a key parameter in our missing marker handling step. We will optimize its value, described in Section 4.3.

4.2 Noisy Trajectory Smoothing

Besides the aforementioned missing marker issue, the original butterfly mocap data are often noisy. This is largely due to the fast flapping motion of butterflies. To this end, in this work we adopt the Savitzky-Golay (S-G) filter [Schafer 2011] to denoise the captured butterfly motion data. The core idea of the S-G filter is to perform a fitting with a polynomial order, k, on multiple continuous frames within a sliding window, n, so as to obtain smoothed results but not disturb the motion tendency. The fidelity of the smoothed motion largely depends on the selection of its key parameters k and n. However, there do not exist standard ways or guidelines to specify

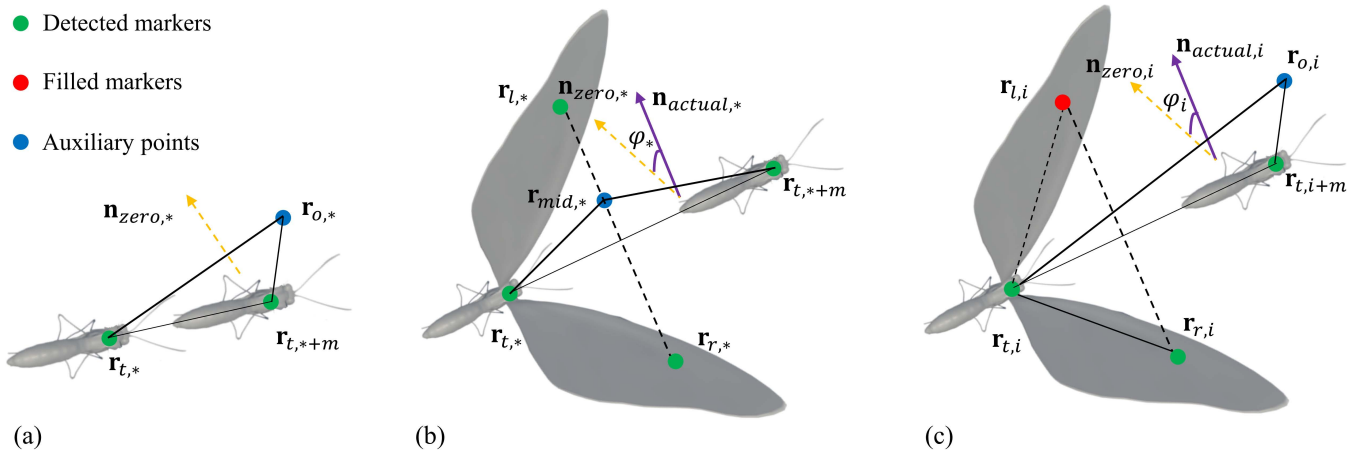

Figure 5: Illustration of the auto-filling process for the missing left wing marker. (a) The reference vertical plane (its normal denoted by $\mathbf{n}_{zero,*}$) of the butterfly's body with a zero roll angle φ at any frame. (b) The roll angle φ_* between the actual-posture-plane (its normal denoted by $\mathbf{n}_{actual,*}$) and the reference vertical plane (its normal denoted by $\mathbf{n}_{zero,*}$). (c) The missing left wing marker (red point) at the i-th frame can be filled with the aid of $\mathbf{n}_{zero}$, $\mathbf{n}_{actual}$, and φ_i. φ_i is computed through a cubic spline interpolation of the φ_* of fully captured, neighboring frames (refer to (b)).

the optimal values for k and n in the S-G filter. As described in Section 4.3, we optimize the values of the key parameters k and n in the S-G filter, besides the m parameter in the above missing marker handling step.

4.3 Key Parameters Optimization

As mentioned above, there are three key parameters (that is, the step size m, the polynomial order k, and the sliding window size n) in our butterfly motion processing steps. Empirically choosing their values may lead to less accurate butterfly motion. In this section, we introduce a method to automatically optimize the values of the three key parameters.

Specifically, we employ a genetic algorithm (GA) to find the optimal values for m, n, and k. We first select a portion of the fully captured butterfly motion data (that is, the used butterfly motion was fully captured, without missing markers) as the ground-truth data in our optimization process. Also, we need to introduce a metric to evaluate the accuracy achieved by combinations of different parameter values.

An error ϵ is defined between the ground-truth data and the filled (processed) data by our method that uses specific values for the three key parameters, and it is calculated as follows:

$$\epsilon_i = \sum_{*\in\{l,r\}} \left|\mathbf{r}_{w_*,i} - \widehat{\mathbf{r}}_{w_*,i}\right|, \tag{5}$$

where $\widehat{\mathbf{r}}_{w_*,i}$ denotes the processed marker $\mathbf{r}_{w_*}$ at the i-th frame by our method. $\mathbf{r}_{w_l}$ and $\mathbf{r}_{w_r}$ denote the markers on the left and right wings, respectively.

Then, an objective function q based on ϵ is further defined to calculate the fitness value, which is computed as follows:

$$q = 1/\left(\frac{1}{N}\sum_{i=1}^{N}\epsilon_i\right), \tag{6}$$

where N is the total number of frames in the used ground-truth data.

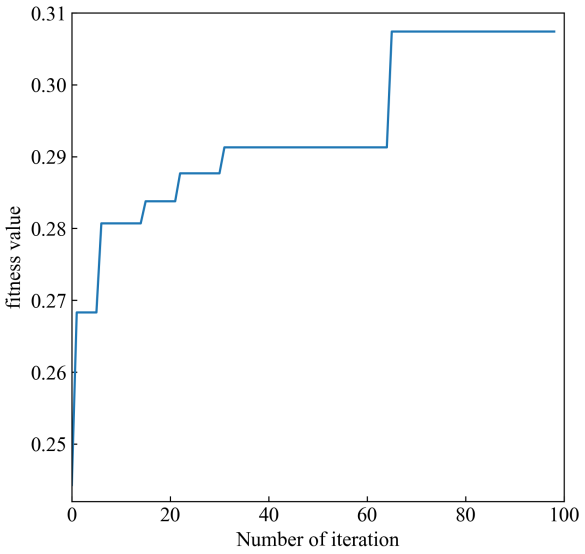

Figure 6: The change of the fitness value q over iterations in our parameters optimization process.

In the GA algorithm, the fitness value q measures the quality of different combinations. Specifically, we use 20 individuals per generation. The reproduction parameters used are a 2% mutation probability and a 92% crossover probability. Each optimization is designed to iterate for 100 generations. Then, the optimal values of the three parameters are iterated with the goal of improving q. We plot the change of q over iterations in Figure 6. As shown in this figure, q achieves the highest value 0.307 with 65 iterations when

the optimal values of the key parameters are: $m = 8$, $n = 19$, and $k = 13$.

5 RESULTS AND COMPARISONS

We used the obtained butterfly motion data to drive a virtual butterfly model to generate animations, meanwhile we draw the trajectory of the virtual markers on the butterfly model (shown in Figure 1(c)). For more butterfly animations driven by our captured motion data, please refer to the supplemental video.

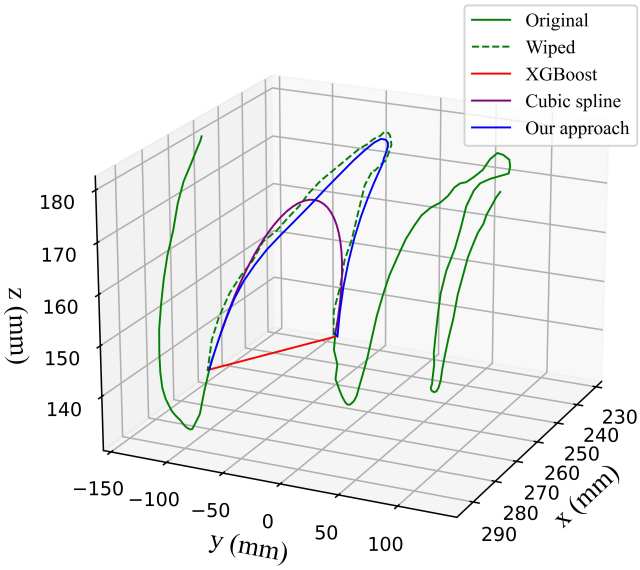

Figure 7: Comparisons between our method and existing methods. The wiped data (green dashed) denotes a randomly selected portion of the ground-truth data that is intentionally removed for this comparison purpose.

5.1 Comparisons

To evaluate the effectiveness of our butterfly motion processing method (Section 4), we also compared our method with two existing, well-known motion interpolation/processing methods: (i) the *cubic spline interpolation* that is considered as one of the most practical and widely used interpolation methods in mocap tasks [Liu and McMillan 2006], and (ii) the *XGBoost* method that is one of popular boosting tree algorithms for data fitting with small datasets [Lisca et al. 2021; Wang et al. 2020]. To perform this comparison, we selected some fully captured butterfly motion data in our dataset (in other words, the selected butterfly motion data do not need any motion post-processing) and then randomly removed some portions of the left wing marker data. Then, we applied the three methods (cubic spline interpolation, XGBoost, and our approach) to fill the positions of the missing left wing marker in our selected data.

Qualitative comparison. We conducted a qualitative comparison among the three methods. Figure 7 shows the visualization of example results by the three methods. As clearly shown in this figure, our method can fill significantly more accurate butterfly motion than the other two methods (cubic spline interpolation, and XGBoost). Arguably, the main reason is that, our motion processing method is specifically designed for butterfly motion and takes full advantage of the spatial characteristics of butterfly flights; therefore, it has significant advantages over the other two methods.

Quantitative comparison. We also used the error metric ϵ (defined in Equation 5) to quantitatively compare our butterfly motion processing method with the aforementioned two methods. The average errors achieved by the three methods on our data are: 18.04 mm (cubic spline interpolation), 37.95 mm (XGBoost), and 4.11 mm (our method). From the above comparison of the average errors, our motion processing method specifically designed for butterfly motion processing has significant edges over both the classical cubic spline interpolation method and the XGBoost method.

6 BUTTERFLY MOTION DATASET

In this work, based on our proposed butterfly motion capure approach, we created a first-of-its-kind butterfly motion dataset, and plan to make it publicly available (*https://github.com/ButterflyDataset/butterflymotiondatasets.git*) to the research community after this publication. In this section we briefly describe this unique butterfly motion dataset.

Our butterfly motion dataset contains 18 flights from 5 different butterflies. Table 2 summarizes main flight characteristics (including flapping frequency/amplitude, undulation frequency/amplitude, and velocity) of 6 selected butterfly flight motions, as well as the statistics of all the flight motions in our dataset.

Based on the acquired butterfly motion data, we found that the frequencies of the undulating motion of the butterfly body are consistent with the flapping frequencies, suggesting that the wing motion and the body motion are closely coupled to each other. The butterfly body is pulled up during the wing down-stroke and undulates with a phase offset with wing motion.

Our quantitative analysis on the butterfly motion further reveals the following findings:

- The flapping wing frequencies of butterflies remain fairly confined between 8 and 12 Hz.
- The amplitudes of wing flapping vary significantly with the average = 154°.
- The undulation frequencies of the butterfly body are similar to the flapping frequencies of butterfly wings.
- The average amplitude of body undulations is $2.82mm$.
- The average flight speed of butterflies is $1.20m/s$.

Butterfly trajectories and velocities. Figure 8(a) shows the thorax trajectory of a butterfly during four flapping cycles with a left turn and horizontal flight motion. The velocity components of the thorax marker are shown in Figure 8(b). The vertical velocity component v_y shows prominent oscillations, compared to other velocity components.

Figure 9(a) shows a trajectory of the butterfly body and its undulation. Figure 9(b) shows the body oscillations that are calculated by subtracting the mean vertical positions from the original data. In this way, users can extract flight characteristics from multiple butterfly flight trajectories.

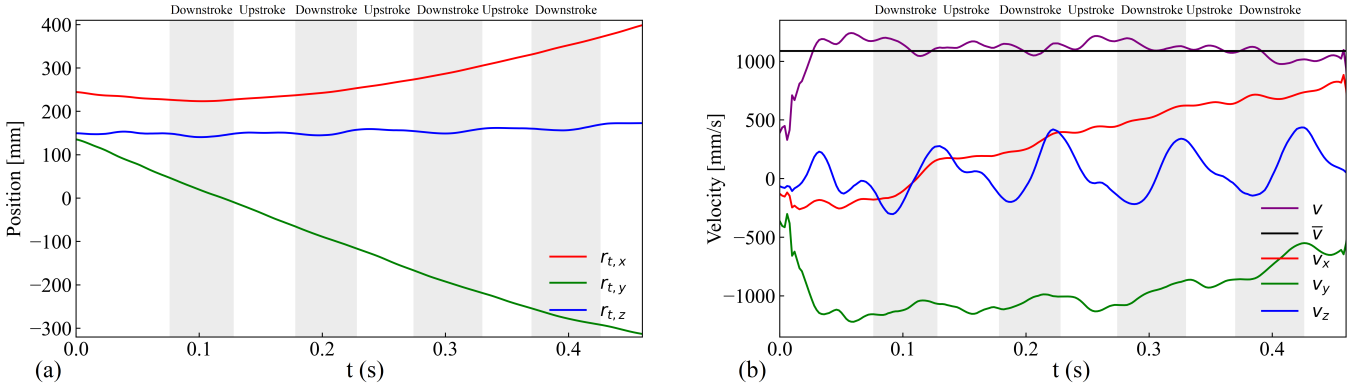

Figure 8: (a) XYZ positions of the thorax marker over time during a butterfly flight. (b) The velocity components of the thorax marker. The velocity magnitude, v, and its average $\bar{v}$ are also plotted.

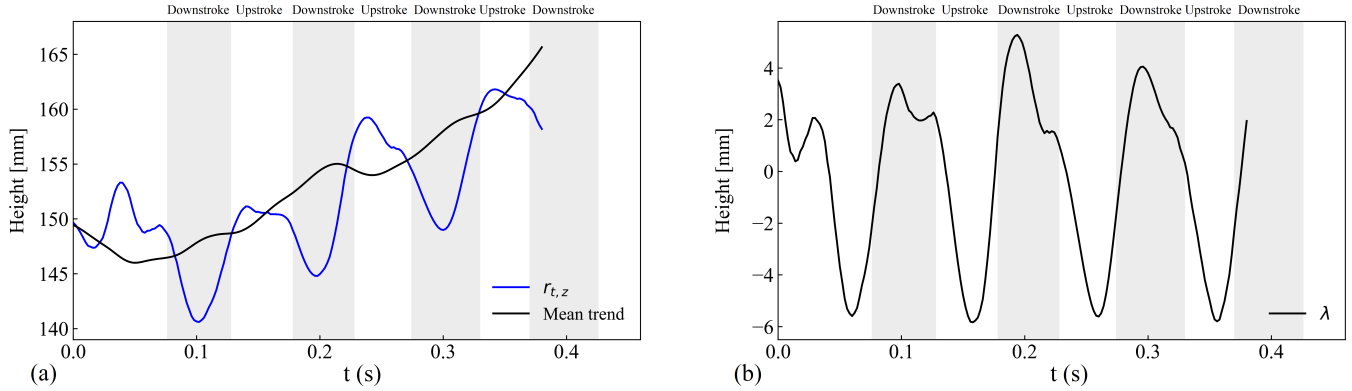

Figure 9: Butterfly body undulation as a function of time. (a) Vertical positions of the butterfly body and its mean trend; (b) butterfly body oscillations around the mean trend, calculated by subtracting the mean trend of the vertical positions from the original data.

Table 2: Means and standard deviations of some main characteristics of 6 selected butterfly flight motions in our dataset, as well as the statistics of all the butterfly flight motions in our dataset (bottom row)

Flight #	Length [s]	Flapping Frequency [Hz]	Flapping Amplitude [°]	Undulation Frequency [Hz]	Undulation Amplitude [mm]	Velocity [m/s]
2	0.49	10.24	187.95	10.15	3.13	1.16
5	0.47	10.74	148.28	10.74	2.79	1.13
7	0.48	10.35	151.01	10.25	2.79	1.21
11	0.63	11.05	134.25	11.05	2.59	1.09
12	0.45	11.12	170.77	11.16	2.91	1.41
15	0.34	8.72	133.91	8.75	2.73	1.17
Total	0.48 ± 0.09	10.37 ± 0.88	154.36 ± 21.30	10.35 ± 0.88	2.82 ± 0.18	1.20 ± 0.11

Flapping angles. We found that the flapping angles of the butterfly exhibit an approximately sinusoidal behavior. An example of flapping angle traces is shown in Figure 10(a). The flapping angle β does not go to zero in all our butterfly motion data, suggesting that the butterfly wings do not touch each other during flights. The average amplitude of the flapping motion is about 148°.

Body angles. Body angles are computed at each time. The pitch angle of the butterfly body, θ, which is the angle between the thorax and the horizontal plane, varies between −19.1° and 32.7°. The pitch angles of the butterfly body show a periodic oscillation similar to the flapping angles, β, but with a small phase difference. Other Euler angles of the butterfly body in four flapping cycles are also shown in Figure 10(b).

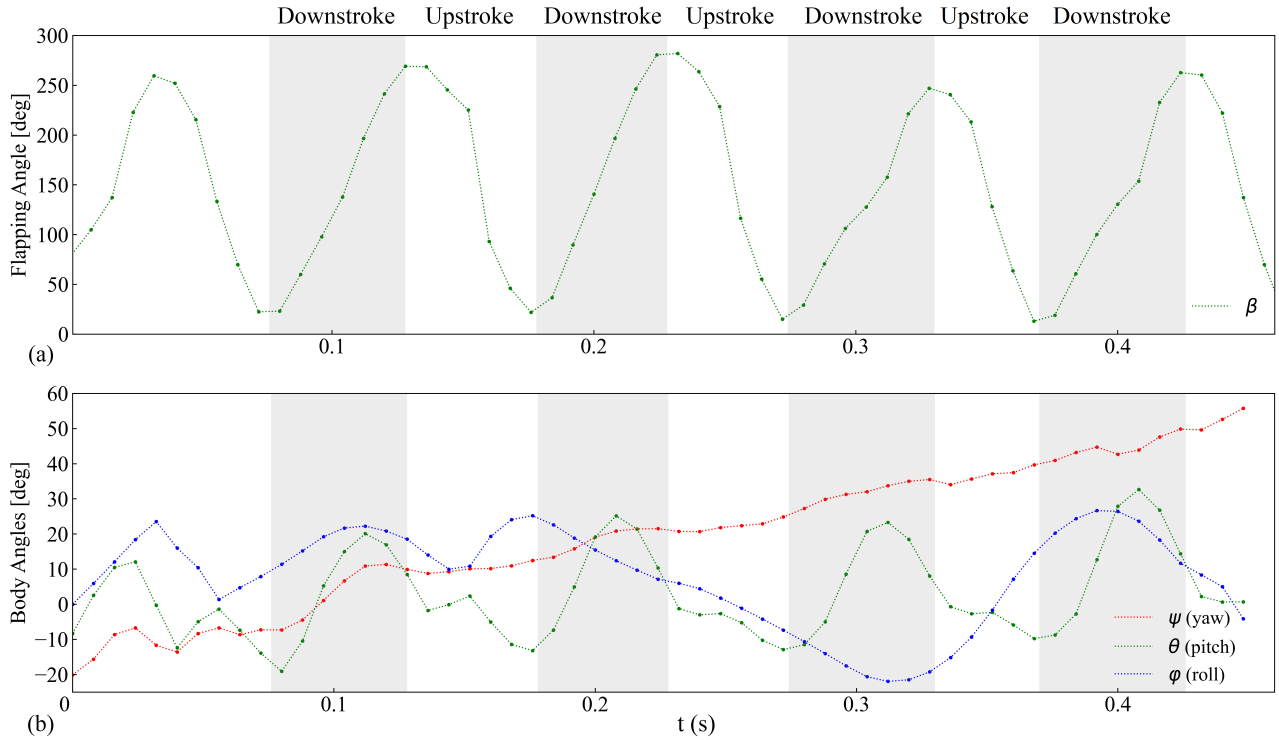

Figure 10: (a) The butterfly flapping angles β over cycles; (b) The yaw angles ψ, pitch angles θ, and roll angles φ of the butterfly.

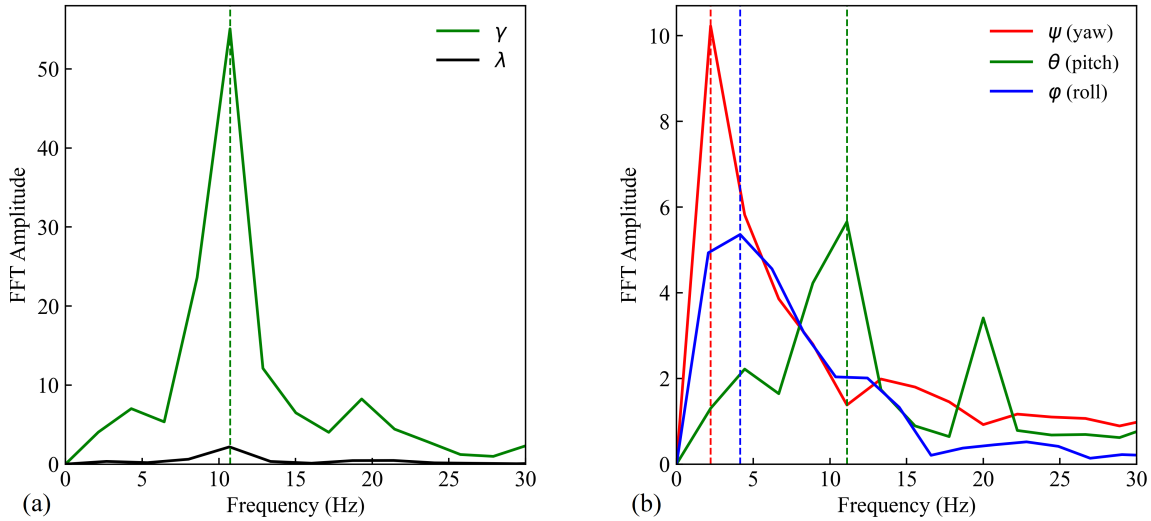

Figure 11: Results of the Fast Fourier Transform performed on flapping angles and body undulations (a), and the Euler angles of the butterfly body (b).

Frequencies. Dominant frequencies of the wing angles, body angles, and body undulations are obtained through Fast Fourier Transform (FFT). Figure 11 shows FFT analysis results of the wing angles, body angles, and body undulations. Interestingly, from our FFT analysis, we found that the flapping angles and the body undulations show the same dominant frequency at $f = 10.74$ Hz (Figure 11(a)). Similarly, we found that the pitch angles of the butterfly body have a similar frequency (11.10Hz) as that of the flapping motion. In contrast, the yaw and roll angles of the butterfly body show peaks at 2.22 Hz and 4.16 Hz, respectively. The pitch angles, unlike other angles, have two peaks within a stroke as shown in Figure 11(b) consistent with the observation in Figure 10(b).

7 DISCUSSION AND CONCLUSION

In this paper we present a practical method for butterfly motion capture, based on an off-the-shelf optical motion capture system. Due to the fast flapping of butterflies, the directly captured butterfly motion data often contain missing markers or errors. To this end, we propose a series of butterfly-specific motion processing steps including missing marker handling and trajectory smoothing, with GA-optimized key parameters. Through comparisons with existing motion interpolation methods including cubic spline interpolation and XGBoost algorithms, we demonstrate our method can produce more accurate butterfly motions. Besides swallow-tail butterfly (*Papilio polytes*) in this paper, the proposed approach can be used to capture motions of other butterfly species. In addition, we will publicly release the captured butterfly flight motion dataset (containing 18 flights from 5 different butterflies) to the research community.

Although in this work we demonstrate the effectiveness of our current approach through various comparisons and analysis, our method still has several limitations, described below.

- Limited by the sensing capability of the used optical motion capture system, the volume for butterfly motion capture is confined in a cylinder-shape space, where the radius is about 1.0 meter and height is about 1.0 meter. Therefore, the maximum duration of captured butterfly flight motions is limited to 0.63 second, which is still longer than the butterfly duration reported by previous methods [Sridhar et al. 2016].
- In this work, we treat the bilateral wings flapping of the butterfly with synchronous frequencies[Dudley 2002]. However, due to the complex aerodynamics and wing structure of the butterfly, the butterfly wings' deformation may not be absolutely symmetric. In the future, we plan to conduct more experiments to capture the butterfly wings' motion with respect to deformation influence.

ACKNOWLEDGMENTS

Qiang Chen was supported in part by the China NSFC (Grant No. 62262024), Scientific Research Project of Education Department of Jiangxi Province (Grant Nos. GJJ210511, GJJ207109). Yuming Fang was supported in part by China NSFC (Grant No. 62132006) and Shenzhen Municipal Science and Technology Innovation Council (Grant No. 2021Szvup051). Zhigang Deng was in part supported by US NSF IIS-2005430.

REFERENCES

Bobby Bodenheimer, Chuck Rose, Seth Rosenthal, and John Pella. 1997. The process of motion capture: Dealing with the data. In *Computer Animation and Simulation'97*. Springer, 3–18.

Kang Chen, Yupan Wang, Song-Hai Zhang, Sen-Zhe Xu, Weidong Zhang, and Shi-Min Hu. 2021. MoCap-Solver: A neural solver for optical motion capture data. *ACM Transactions on Graphics (TOG)* 40, 4 (2021), 1–11.

Qiang Chen, Tingsong Lu, Yang Tong, Guoliang Luo, Xiaogang Jin, and Zhigang Deng. 2022. A Practical Model for Realistic Butterfly Flight Simulation. *ACM Transactions on Graphics (TOG)* 41, 3 (2022), 1–12.

Qiang Chen, Guoliang Luo, Yang Tong, Xiaogang Jin, and Zhigang Deng. 2019. Shape-constrained flying insects animation. *Computer Animation and Virtual Worlds* 30, 3-4 (2019), e1902.

Michael H Dickinson, Fritz-Olaf Lehmann, and Sanjay P Sane. 1999. Wing rotation and the aerodynamic basis of insect flight. *Science* 284, 5422 (1999), 1954–1960.

Robert Dudley. 2002. *The biomechanics of insect flight: form, function, evolution.* Princeton University Press.

SN Fry, M Bichsel, P Müller, and D Robert. 2000. Tracking of flying insects using pan-tilt cameras. *Journal of Neuroscience Methods* 101, 1 (2000), 59–67.

Yang-yang Guo, Dong-jian He, and Cong Liu. 2018. Target tracking and 3D trajectory acquisition of cabbage butterfly (P. rapae) based on the KCF-BS algorithm. *Scientific Reports* 8, 1 (2018), 1–13.

Daniel Holden. 2018. Robust solving of optical motion capture data by denoising. *ACM Transactions on Graphics (TOG)* 37, 4 (2018), 1–12.

Tatjana Y Hubel, Nickolay I Hristov, Sharon M Swartz, and Kenneth S Breuer. 2009. Time-resolved wake structure and kinematics of bat flight. *Experiments in Fluids* 5, 46 (2009), 933–943.

Benjamin Jantzen and Thomas Eisner. 2008. Hindwings are unnecessary for flight but essential for execution of normal evasive flight in Lepidoptera. *Proceedings of the National Academy of Sciences* 105, 43 (2008), 16636–16640.

LC Johansson and P Henningsson. 2021. Butterflies fly using efficient propulsive clap mechanism owing to flexible wings. *Journal of the Royal Society Interface* 18, 174 (2021), 20200854.

Eunjung Ju, Jungdam Won, Jehee Lee, Byungkuk Choi, Junyong Noh, and Min Gyu Choi. 2013. Data-driven control of flapping flight. *ACM Transactions on Graphics (TOG)* 32, 5 (2013), 1–12.

Christopher Koehler, Thomas Wischgoll, Haibo Dong, and Zachary Gaston. 2011. Vortex visualization in ultra low Reynolds number insect flight. *IEEE transactions on visualization and computer graphics* 17, 12 (2011), 2071–2079.

Weizi Li, David Wolinski, Julien Pettré, and Ming C. Lin. 2015. Biologically-inspired visual simulation of insect swarms. In *Computer Graphics Forum*, Vol. 34. Wiley Online Library, 425–434.

Gheorghe Lisca, Cristian Prodaniuc, Thomas Grauschopf, and Cristian Axenie. 2021. Less Is More: Learning Insights From a Single Motion Sensor for Accurate and Explainable Soccer Goalkeeper Kinematics. *IEEE Sensors Journal* 21, 18 (2021), 20375–20387.

Guodong Liu and Leonard McMillan. 2006. Segment-based human motion compression. In *Proceedings of the 2006 ACM SIGGRAPH/Eurographics symposium on Computer animation*. 127–135.

Matthew Loper, Naureen Mahmood, and Michael J Black. 2014. MoSh: Motion and shape capture from sparse markers. *ACM Transactions on Graphics (ToG)* 33, 6 (2014), 1–13.

Thomas B Moeslund and Erik Granum. 2001. A survey of computer vision-based human motion capture. *Computer vision and image understanding* 81, 3 (2001), 231–268.

AB Qualisys. 2013. Packhusgatan 6, 411 13 Gothenburg. *Sweden, Qualisys Track Manager Manual* (2013).

Leif Ristroph, Attila J Bergou, John Guckenheimer, Z Jane Wang, and Itai Cohen. 2011. Paddling mode of forward flight in insects. *Physical review letters* 106, 17 (2011), 178103.

Ronald W. Schafer. 2011. What Is a Savitzky-Golay Filter? *IEEE Signal Processing Magazine* 28, 4 (2011), 111–117.

Michael Sinhuber, Kasper Van Der Vaart, Rui Ni, James G Puckett, Douglas H Kelley, and Nicholas T Ouellette. 2019. Three-dimensional time-resolved trajectories from laboratory insect swarms. *Scientific data* 6, 1 (2019), 1–8.

Madhu Sridhar, Chang-Kwon Kang, and D Brian Landrum. 2016. Instantaneous lift and motion characteristics of butterflies in free flight. In *46th AIAA Fluid Dynamics Conference*. 3252.

RB Srygley and ALR Thomas. 2002. Unconventional lift-generating mechanisms in free-flying butterflies. *Nature* 420, 6916 (2002), 660–664.

Daniel Vlasic, Rolf Adelsberger, Giovanni Vannucci, John Barnwell, Markus Gross, Wojciech Matusik, and Jovan Popović. 2007. Practical motion capture in everyday surroundings. *ACM transactions on graphics (TOG)* 26, 3 (2007), 35–es.

Chao Wang, Peter P. K. Chan, Ben M. F. Lam, Sizhong Wang, Janet H. Zhang, Zoe Y. S. Chan, Rosa H. M. Chan, Kevin K. W. Ho, and Roy T. H. Cheung. 2020. Real-Time Estimation of Knee Adduction Moment for Gait Retraining in Patients With Knee Osteoarthritis. *IEEE Transactions on Neural Systems and Rehabilitation Engineering* 28, 4 (2020), 888–894.

Xinjie Wang, Xiaogang Jin, Zhigang Deng, and Linling Zhou. 2014. Inherent noise-aware insect swarm simulation. In *Computer Graphics Forum*, Vol. 33. Wiley Online Library, 51–62.

Xinjie Wang, Jiaping Ren, Xiaogang Jin, and Dinesh Manocha. 2015. BSwarm: biologically-plausible dynamics model of insect swarms. In *Proceedings of the 14th ACM SIGGRAPH/Eurographics Symposium on Computer Animation*. 111–118.

Wei Xiang, Xinran Yao, He Wang, and Xiaogang Jin. 2020. FASTSWARM: A data-driven framework for real-time flying insect swarm simulation. *Computer Animation and Virtual Worlds* 31, 4-5 (2020), e1957.

Qian Yu, Qing Li, and Zhigang Deng. 2007. Online motion capture marker labeling for multiple interacting articulated targets. In *Computer Graphics Forum*, Vol. 26. Wiley Online Library, 477–483.